CHEMISTRY OF MATERIALS

Article

pubs.acs.org/cm

Interaction of Organic Cation with Water Molecule in Perovskite $MAPbI_3$: From Dynamic Orientational Disorder to Hydrogen Bonding

Zhuan Zhu,[†,‡] Viktor G. Hadjiev,[§,∥] Yaoguang Rong,[†] Rui Guo,[†,⊥] Bo Cao,[#] Zhongjia Tang,[■] Fan Qin,[●] Yang Li,[†] Yanan Wang,[†,‡] Fang Hao,[†] Swaminathan Venkatesan,[†] Wenzhi Li,[⊥] Steven Baldelli,[■] Arnold M. Guloy,[■] Hui Fang,[▲] Yandi Hu,[#] Yan Yao,[†,§,●] Zhiming Wang,[*,‡] and Jiming Bao[*,†,‡,■,●,▼]

[†]Department of Electrical and Computer Engineering, [§]Texas Center for Superconductivity, [∥]Department of Mechanical Engineering, [#]Department of Civil and Environmental Engineering, [■]Department of Chemistry, [●]Materials Engineering Program, and [▼]Center for Advanced Materials, University of Houston, Houston, Texas 77204, United States

[‡]Institute of Fundamental and Frontier Sciences, University of Electronic Science and Technology of China, Chengdu, Sichuan 610054, China

[⊥]Department of Physics, Florida International University, Miami, Florida 33199, United States

[▲]Department of Physics, Sam Houston State University, Huntsville, Texas 77341, United States

Supporting Information

ABSTRACT: Microscopic understanding of interaction between H_2O and $MAPbI_3$ ($CH_3NH_3PbI_3$) is essential to further improve efficiency and stability of perovskite solar cells. A complete picture of perovskite from initial physical uptake of water molecules to final chemical transition to its monohydrate $MAPbI_3{\cdot}H_2O$ is obtained with in situ infrared spectroscopy, mass monitoring, and X-ray diffraction. Despite strong affinity of MA to water, $MAPbI_3$ absorbs almost no water from ambient air. Water molecules penetrate the perovskite lattice and share the space with MA up to one H_2O per MA at high-humidity levels. However, the interaction between MA and H_2O through hydrogen bonding is not established until the phase transition to monohydrate where H_2O and MA are locked to each other. This lack of interaction in water-infiltrated perovskite is a result of dynamic orientational disorder imposed by tetragonal lattice symmetry. The apparent inertness of H_2O along with high stability of perovskite in an ambient environment provides a solid foundation for its long-term application in solar cells and optoelectronic devices.

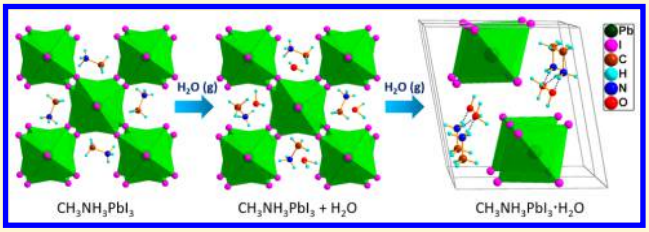

INTRODUCTION

Organic−inorganic hybrid perovskite $CH_3NH_3PbI_3$ ($MAPbI_3$) has shown great potential for high-efficiency low-cost solar cells and optoelectronic devices, but its chemical stability in ambient environments has hindered large-scale commercial application.[1−8] $MAPbI_3$ was found to be very sensitive to the environment, especially to water or moisture: the dark film of $MAPbI_3$ turned yellow because of its decomposition to PbI_2.[9−12] Early proposal indicates that even a single water molecule can catalyze the degradation of perovskite to PbI_2.[7,13,14] Later, two groups used X-ray diffraction (XRD) and claimed perovskite dihydrate $(MA)_4PbI_6{\cdot}2H_2O$ as an intermediate phase before decomposition.[15,16] Shortly after that, Leguy et al. reported that the perovskite first became monohydrate $MAPbI_3{\cdot}H_2O$ before further hydration to $(MA)_4PbI_6{\cdot}2H_2O$.[17] The observation of monohydrate in the degradation pathway is very convincing, but it is still not well-recognized in recent literature.[3,8] In the meantime, first-principles calculation and molecular dynamics were employed to gain microscopic understanding of degradation pathways and the atomic interaction between perovskite and water molecules.[18−20] These simulations show that water molecules can spontaneously permeate into perovskite lattice and form hydrogen bonds with MA cations and iodine ions.[18,21] Recent experiments studied the effect of moisture on the electronic and lattice structures of perovskite.[20−22] Grancini et al. observed a blue shift in photoluminescence and changes to MA Raman spectrum when single-crystal perovskite was exposed to moisture, and attributed them to the widening of band gap and formation of hydrogen bonding of MA with water.[20] Müller et al. observed a uniform red shift by ∼10 cm^{-1} in the infrared (IR) spectrum of MA, and also attributed the shift to the hydrogen bonding. They further showed that the perovskite film became saturated by water molecules with 2:1 $MAPbI_3/H_2O$ molar ratio even at 10% low relative humidity (RH).[21] However, different from Grancini et al.'s work,[20] their IR results show negligible water absorption in perovskite single crystal at ambient conditions (∼40% RH).[21]

In this work, we present a very different but more complete picture of interaction of water with perovskite using first-

Received: July 14, 2016
Revised: September 6, 2016
Published: September 21, 2016

DOI: 10.1021/acs.chemmater.6b02883
Chem. Mater. 2016, 28, 7385−7393

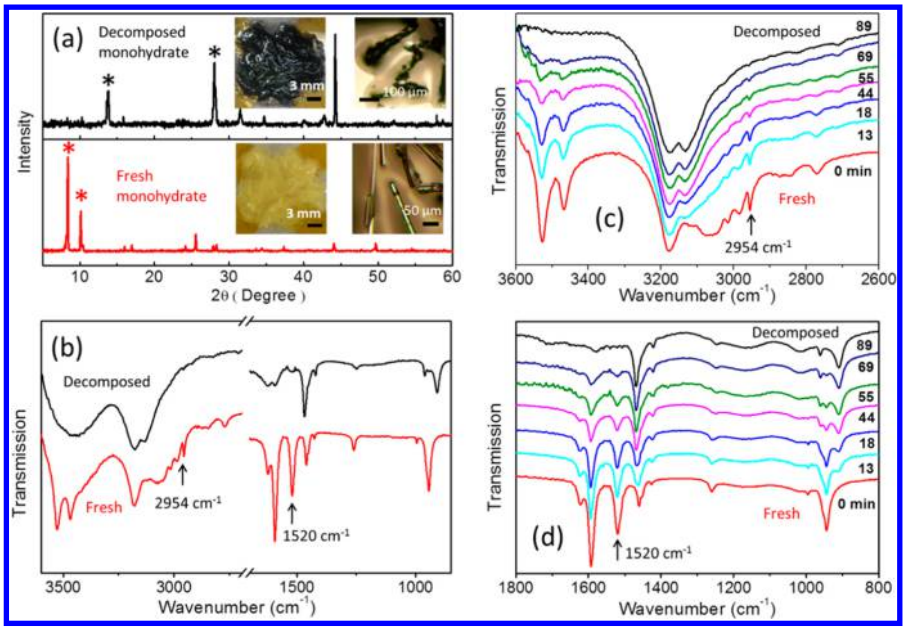

Figure 1. XRD patterns and FTIR spectra of fresh and decomposed perovskite monohydrate $MAPbI_3·H_2O$. (a) XRD patterns. Insets are optical macroscopic and microscopic images. Decomposed monohydrate was obtained by brief N_2 flushing in air. (b) Corresponding FTIR spectra by attenuated total reflection (ATR). (c, d) Evolution of ATR FTIR spectrum of perovskite monohydrate as it was exposed to ambient air.

principles vibrational dynamics and a comprehensive set of techniques which enable us to monitor in situ the lattice vibrations, lattice structure, and moisture uptake when perovskite is exposed to an environment with controlled humidity. After confirmation of monohydrate as the immediate hydrate of perovskite and their reversible transition by XRD, we show that the hydration of perovskite is very different from dehydration of monohydrate with Fourier transform infrared spectroscopy (FTIR). Contrary to some misunderstandings and previous reports, water absorption in ambient air (25 °C and 40−45% RH) is negligible; significant water absorption is observed only when the RH reaches ∼85%, with the maximum 1:1 $MAPbI_3/H_2O$ molar ratio at RH of ∼100%. We show direct evidence that water molecules are not simply adsorbed on the surface or trapped in grain boundaries; they penetrate the lattice and fill the space surrounded by PbI_6 cages with MA without changing the tetragonal lattice structure and MA vibration spectrum. We identify a set of distinctive IR bands that serve as "fingerprints" of the onset of hydrogen bonding between H_2O and MA. These fingerprints allow us to monitor the phase transition from water-saturated perovskite where MA cations and water molecules are orientationally disordered to monohydrate $MAPbI_3·H_2O$ where they are locked to each other through hydrogen bonding. The inactivity of water molecules with perovskite is further supported by our observation of superior chemical stability of $MAPbI_3$ in ambient conditions when it is stored in the dark.

RESULTS

Infrared Spectrum of $MAPbI_3·H_2O$. We start first by confirming that monohydrate $MAPbI_3·H_2O$, rather than dihydrate $(MA)_4PbI_6·2H_2O$, is the first hydrated phase of $MAPbI_3$.[17,23,24] To achieve this, we synthesized $MAPbI_3·H_2O$ following a reported hydrothermal method.[17,24,25] Figure 1a shows optical images and X-ray diffractions of fresh monohydrate and its dehydrated product by brief nitrogen blowing in ambient air. The initial pale yellow material of $MAPbI_3·H_2O$ can be recognized by characteristic XRD peaks at 8.35° and 10.31°, and the dark dehydrated product is confirmed as $MAPbI_3$ by strong XRD diffraction peaks at 14.18° and 28.46°.[17,24] The optical images also reveal that monohydrate consists of microwires with uniform diameter, but the structure collapses after dehydration.[24] XRD confirmed that yellow monohydrate reappeared when such-obtained dark perovskite was exposed to moist N_2 (RH > 95%), although single-crystal microwires are not recovered.

The establishment of reversible transition between $MAPbI_3·H_2O$ and $MAPbI_3$ enables us to obtain vibrational spectrum of $MAPbI_3·H_2O$ and use it to further study the phase transition. Figure 1b shows IR spectra of fresh and dehydrated $MAPbI_3·H_2O$ as in Figure 1a. A significant difference can be seen between two spectra, and the spectrum of $MAPbI_3$ (dehydrated monohydrate) is nearly identical to those reported before except a broad water absorption band near 3450 cm^{-1}.[26,27] This broad band is also present in the spectrum of fresh monohydrate, and is due to residue water initially adsorbed to fresh monohydrate when it was extracted from reaction solution. To unambiguously identify major IR features of monohydrate, we prepared dry monohydrate with much less surface water residue, and then let it degrade slowly in ambient air and monitored the transition with FTIR. Figure 1c,d shows the evolution of IR spectrum as the fresh monohydrate dehydrated and became perovskite in about 89 min. The major changes in spectrum can be summarized as follows from high to low wavenumber: (1) The disappearance of two sharp peaks near 3500 cm^{-1}; (2) asymmetric stretching mode of NH_3^+ remaining the same, but several peaks in the 3000 cm^{-1} region disappearing accompanied by the emergence of the symmetric stretching mode of NH_3^+ at 3133 cm^{-1}; (3) two modes in the 1500 cm^{-1} region disappearing; (4) spectral shifts for three peaks in the region of 1300−900 cm^{-1}. It can also be seen that the broad water absorption band near 3500 cm^{-1} is not so visible in both fresh and degraded monohydrate due to the elimination of water residue.

DOI: 10.1021/acs.chemmater.6b02883
Chem. Mater. 2016, 28, 7385−7393

Signature Molecular Vibration Modes of $MAPbI_3·H_2O$ by First-Principles Calculations. On the basis of the above FTIR observations and first-principles calculations, we are able to identify major IR signatures of $MAPbI_3·H_2O$. Table 1 summarizes the assignment and peak positions of vibrational modes. Similar to the broad water absorption band, the two narrow peaks at 3527 and 3467 cm^{-1} belong to asymmetric and symmetric O−H stretching modes of water. The appearance of the band at 1520 cm^{-1} in Figure 1b,d also correlates with that of the two stretching modes of water. The notable water-related IR feature in monohydrate is the relatively sharp band at 2954 cm^{-1}. This band is of particular significance because it reflects the hydrogen bonding between MA and H_2O that locks otherwise orientationally disordered molecules in PbI_6 cage.

Table 1. Measured Vibrational Modes of Perovskite (Water-Infiltrated Perovskite) and Monohydrate[a]

IR band assignment	$MAPbI_3$ (cm^{-1}) (exp.)	$MAPbI_3·H_2O$ (cm^{-1}) exp.	$MAPbI_3·H_2O$ (cm^{-1}) calc.
$CH_3–NH_3^+$ rock	910	943	952
$CH_3–NH_3^+$ rock	961	955	962
$CH_3–NH_3^+$ stretch		994	1017
$CH_3–NH_3^+$ rock	1248	1260	1277
CH_3 bend	1422	1427	1434
$CH_3–NH_3^+$ bend	1469	1460	1460
H_2O bend		1520	1522*
NH_3^+ bend	1579	1593	1590
NH_3^+ bend		1624	1642
asym. NH_3^+ stretch		2954	2964*
sym. CH_3 stretch	2916	2983	2995
asym. NH_3^+ sym. CH_3 stretch		3075	3042
sym. NH_{3+} stretch	3133		
asym. NH_3^+ stretch	3176	3176	3253*
sym. H_2O stretch		3467	3466*
asym. H_2O stretch		3526	3520*

[a]The asterisks denote the set of distinctive IR vibrations in monohydrate shown in Figure 2. IR band assignment gives only a crude description of vibrational modes. Additional vibrational eigenvectors of monohydrate are given in the Supporting Information.

Figure 2 displays the three characteristic O−H vibrations of water molecules in $MAPbI_3·H_2O$, calculated[28] [Supporting Information] at 1522, 3466, and 3520 cm^{-1}. The O−H vibrations in the hydrate have lower frequencies than those in water vapor due to the dielectric properties of $MAPbI_3$ cage. In $MAPbI_3·H_2O$, the distance between one of the hydrogen atoms of NH_3^+ and O of neighboring H_2O molecule is 1.93 Å[23]—typical for hydrogen bond lengths. One of the interesting revelations is the pair of vibrational modes at 2964 cm^{-1} (exp. 2954 cm^{-1}) and 3253 cm^{-1} (exp. 3176 cm^{-1}). It involves the same N−H vibrations of the highest frequency doubly degenerate E mode of a free MA molecule split off in $MAPbI_3·H_2O$ to a lower frequency A_u and higher frequency B_u modes. In the A_u mode at 2964 cm^{-1} the H vibration is along the O−H−N hydrogen bond, whereas in the highest frequency B_u mode it is parallel to the H_2O plane. We find this the most distinctive signature for the formation of hydrogen bonds between MA and H_2O. On the other hand, the MA vibration at 3253 cm^{-1} remains unchanged in going from perovskite to monohydrate.

In Situ FTIR Monitoring of Perovskite Hydration and Phase Transition. Although the transformation between $MAPbI_3·H_2O$ and $MAPbI_3$ is reversible, FTIR reveals a big difference in the microscopic process between hydration and dehydration. Figure 3a,b shows the evolution of the FTIR spectrum when the same decomposed monohydrate (perovskite) is exposed to the moist N_2. In contrast to the dehydration process shown in Figure 1c,d, $MAPbI_3·H_2O$ is not formed until about 300 s later despite rapid appearance of water absorption band at 3500 cm^{-1}. This observation indicates that adsorbed water molecules do not transform perovskite to monohydrate immediately, while in the reverse dehydration process, water molecules do not stay with perovskite when monohydrate is decomposed. We also note the concomitant appearance of

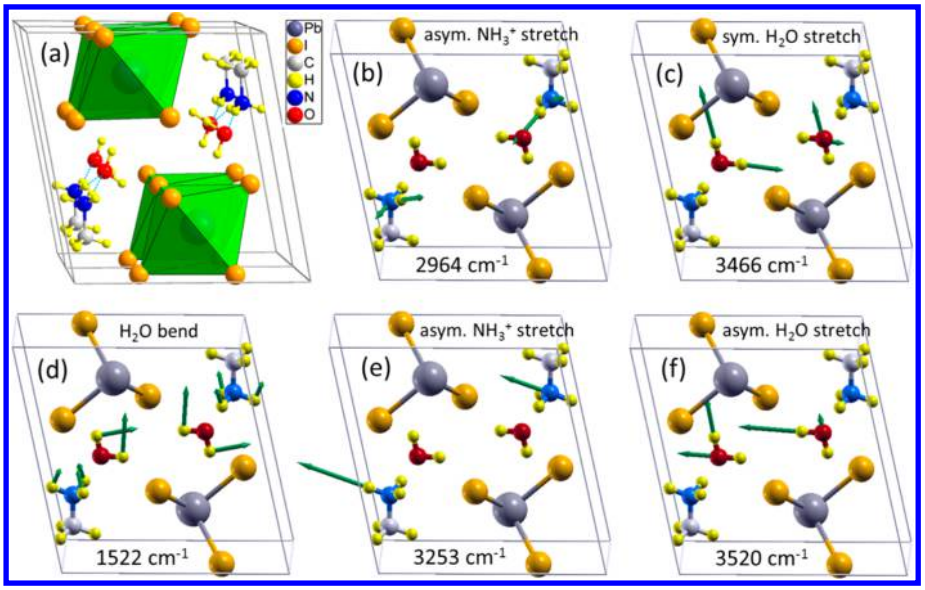

Figure 2. Lattice crystal structure and signature molecular vibrations of $MAPbI_3·H_2O$. (a) Unit cell of lattice crystal structure of $MAPbI_3·H_2O$. Hydrogen bonds between H of NH_3^+ and O of H_2O are indicated by dashed lines. (b–f) Signature molecular vibrations of hydrogen-bonded $CH_3NH_3^+$ and H_2O in $MAPbI_3·H_2O$.

DOI: 10.1021/acs.chemmater.6b02883
Chem. Mater. 2016, 28, 7385−7393

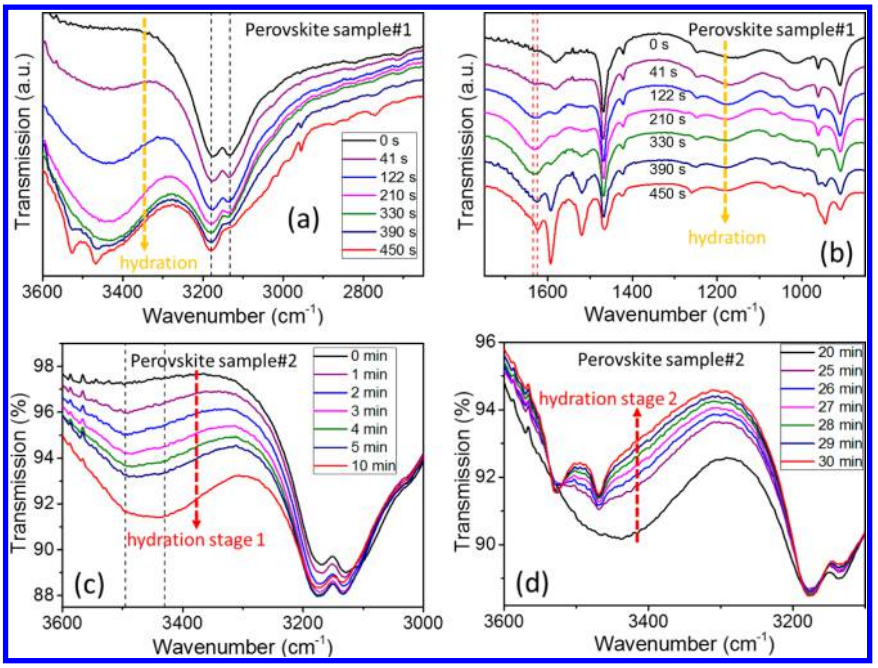

Figure 3. Perovskite hydration and subsequent phase transition to monohydrate in moist N_2 monitored in situ by FTIR. (a, b) The same decomposed monohydrate (perovskite) as in Figure 1c,d. (c, d) Powders of perovskite single crystal. Black and red solid curves stand for the start and end in each figure, respectively. Relative humidity (RH) > 95%.

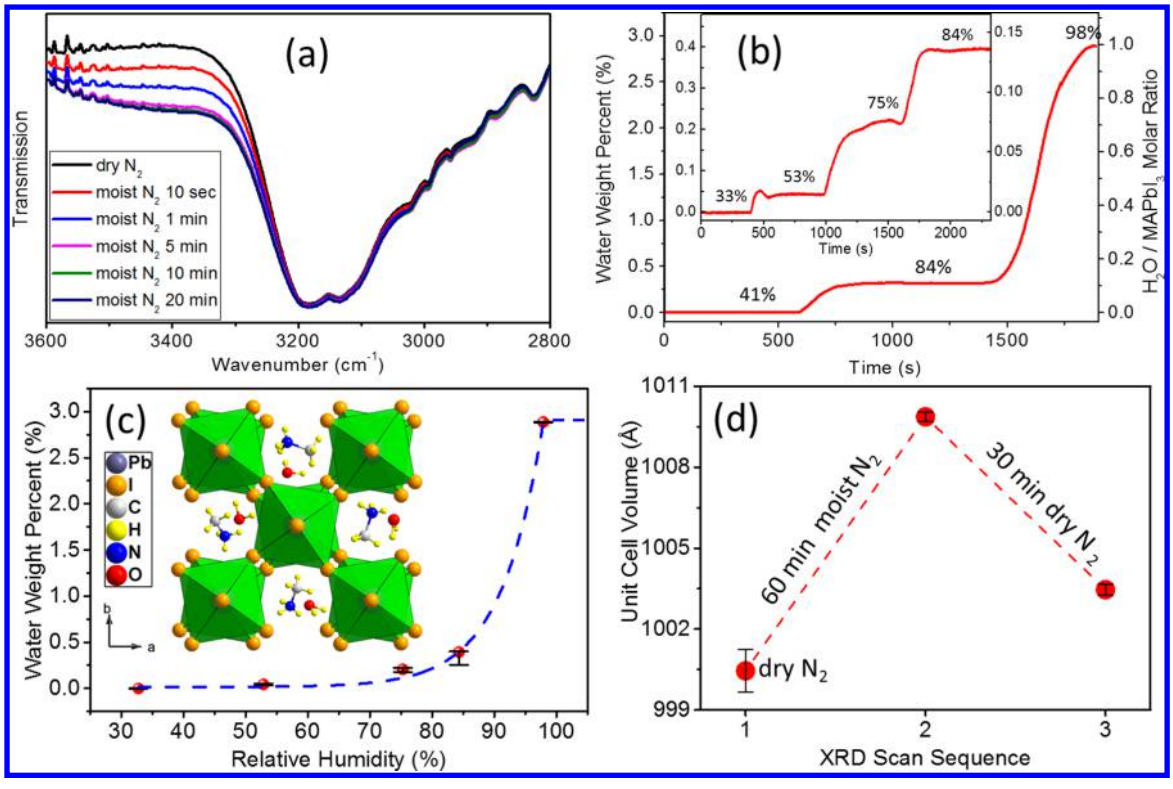

Figure 4. In situ hydration of perovskite thin films monitored by FTIR, XRD, and quartz crystal microbalance with dissipation (QCM-D). (a) Evolution of ATR FTIR spectrum in the same RH level as in Figure 3 (RH > 95%). (b) QCM-D water uptake at increasing RH levels. (c) Water vapor sorption isotherm from (b). Inset shows a schematic of water-infiltrated perovskite when $H_2O/MAPbI_3$ ratio reaches 1:1 at the highest RH level. (d) Change in perovskite unit cell volume when exposed to dry and moist N_2.

absorption band at 1632 cm^{-1}, which is the signature of bending mode of H_2O molecule. The phase transition to monohydrate is marked by the emergence of two sharp peaks on the top of the broad band at 3500 cm^{-1}; the relatively broad 1632 cm^{-1} band also diminishes, along with the appearance of the stronger 1520 cm^{-1} band and the signature 2954 cm^{-1} band. Note that the sharper band at 1624 cm^{-1} involves a NH_3^+ bend mode in the monohydrate.

We can say that the transformation from $MAPbI_3$ to $MAPbI_3 \cdot H_2O$ requires two stages: initial physical water uptake

DOI: 10.1021/acs.chemmater.6b02883
Chem. Mater. 2016, 28, 7385−7393

and subsequent chemical phase transition. These two distinct stages are also observed in single-crystal perovskite. As can be seen from Figure 3c,d, in the first stage, the amount of water increases until the maximum is reached, but once the phase transition starts, the broad band water absorption decreases while the narrow sharp water absorption bands grow, implying that the water in monohydrate comes from the water already adsorbed to perovskite, rather than the surrounding moist environment. It is important to note that, in the water uptake stage before the phase transition, all the IR bands of perovskite remain in the same positions, which is very different from a previous report.[21]

Is there a limit to the amount of water uptake? What is the required minimum amount of water to initiate the phase transition from perovskite to monohydrate? To answer these questions, we turned to perovskite thin film for better quantitative measurement of moisture uptake. Figure 4a shows similar growing broad water absorption band when the perovskite film is exposed to the same moisture environment. The big difference is that water uptake quickly becomes saturated in a few minutes, and there is no more growth and phase transition over the next several hours. We also noted that the water was not observed in the film initially. In fact, as shown in Figure S4a, no difference and no water are observed when a film is exposed to ambient air when taken out from vacuum. Figure S4b even shows no sign of long-term degradation and water absorption when perovskite film is exposed to the ambient air provided that it is kept in the dark. It is worth mentioning that the $MAPbI_3$ film will degrade to PbI_2 slowly if it is left on the benchtop and exposed to room light.[29,30]

Moisture Uptake Measurement by Quartz Crystal Microbalance. To directly monitor and quantify the absorbed water in perovskite, we measure the gain in the mass of the perovskite film using quartz crystal microbalance with dissipation (QCM-D). QCM-D curve in Figure 4b,c confirms that the water absorption happens at a similar rate as before and the total amount of water is limited depending on RH level. At the highest available RH level of ~97%, the mass of the perovskite film increases by 2.9%, corresponding to 1:1 H_2O/$MAPbI_3$ molar ratio. QCM-D also reveals a very surprising observation: the amount of adsorbed water drops very quickly as RH is reduced from the vapor saturation level, by nearly 7 times at the RH of 84%, and negligible water absorption in ambient conditions (Figure S9). Note that, as in Figure 4a, $MAPbI_3{\cdot}H_2O$ is not formed even when the 1:1 $H_2O/MAPbI_3$ molar ratio is reached.

Lattice Expansion Probed by XRD. Water is ubiquitous; its effect on perovskite has been the focus of many studies since the very beginning.[3,4,7,8] It has been suggested that water molecules interact with perovskite through adsorption on the surface or trapping in the grain boundaries.[4,15,17,20] As mentioned before, water is also believed to be able to penetrate the crystal lattice of perovskite;[18−21] however, there is no direct experimental evidence to show any changes to the perovskite lattice. The observation of the maximum water absorption at 1:1 $MAPbI_3/H_2O$ ratio indicates that water molecules do permeate into the lattice structure of perovskite. This conclusion is also supported by the following FTIR and QCM-D measurements using perovskite film with different thicknesses: the amount of water is not determined by the film surface area; instead, it is roughly proportional to the thickness or mass of perovskite films (Table S2 and Figure S3). The final but strongest evidence is given in Figure 4d using unit cell refinement of the entire XRD pattern fitting: the unit cell expands in all three directions with about 1% volume expansion.

DISCUSSION

A microscopic picture of water-saturated perovskite is now obtained (inset of Figure 4c): water molecules and MA cations fill up the space enclosed by PbI_6 octahedrons as in $MAPbI_3{\cdot}H_2O$; the space is even tighter for perovskite because PbI_6 cages there are connected by corner-sharing. The question is why H_2O and MA molecules interact through hydrogen bonding in monohydrate, as manifested by the change to MA vibrational modes, while in perovskite, water has no effect on the MA IR spectrum. This lack of hydrogen bonding in perovskite is surprising, on one hand, because it is in direct contradiction to previous simulations and observation.[18,21] On the other hand, this difference is expected because the dynamics of water and MA molecules in perovskite is different. In monohydrate, the position and orientation of MA and water molecule are locked to each other, as can be seen in Figure 2.[5] This is a general property of stoichiometric hydrates such as gypsum $CaSO_4{\cdot}2H_2O$ (http://www.gmss.us/community/minerals/gypsum).[31] The sharp peaks of stretching and bending modes are a strong indication of isolated and locked water molecules.[31] The situation is different in perovskite. To satisfy the tetragonal lattice symmetry of perovskite, MA and water molecules cannot be locked; as a result, rigid hydrogen bond between H of NH_3 and O of water cannot be established.

It is well-understood that MA cations in perovskite exhibit orientational disorder at room temperature as a consequence of the noncoincidence of the crystallographic site and the molecular cation symmetries.[11,32] This disorder has been confirmed by NMR,[32,33] FTIR,[27] and recently neutron diffraction.[34] The rotation of MA dipole is very fast; neutron scattering measurements show that at room temperature MA ions reorientate between the faces, corners, or edges of the pseudocubic lattice cages every 14 ps.[34] Density functional theory (DFT) calculation reveals that it is such rapid reorientation of MA in many quasi-equivalent directions that transforms the perovskite from an indirect band gap semiconductor to a "dynamical" direct band gap semiconductor.[35]

Note that even when water and MA are locked in perovskite, certain vibration modes such as the asymmetric stretching mode of NH_3^+ at 3253 cm^{-1} remain the same as shown in Figure 2 because this mode does not feel an electrostatic force from the neighboring water molecule. When a polar molecule such as water or MA has dynamic orientational disorder, its net effective or average dipole moment becomes zero. Such weak effective interaction is also observed in several ammonia salts; the stretching vibrations of NH_4^+ are not affected by the surrounding water molecules.[36,37] The orientational disorder of water in perovskite can also be seen from the broad absorption band from water stretching modes. FTIR in Figures S3 and S6 also reveals subtle difference between infiltrated water molecules with those in liquid water or adsorbed on the surface.[38] The absorption band of water stretching modes shifts to lower frequency as the amount of infiltrated water increases.[39,40] The red shift is due to a change in the frequency distribution driven by the increased coupling between O−H stretching vibrations of water molecules,[39,40] frustrated by the limited space in the $MAPbI_3$ cage.

Because of the strong affinity of MA to water, it was believed that water molecules can permeate into perovskite sponta-

DOI: 10.1021/acs.chemmater.6b02883
Chem. Mater. 2016, 28, 7385−7393

neously, or perovskite can uptake water from ambient environment and degrade.[18,19,21] Our observation of weak interaction between water and MA can also be seen from the vapor isotherm curve in Figure 4c. Such curve is typical for hydrophobic crystals.[41] The sharp increase of water uptake and saturation at the phase transition vapor pressure is also characteristic of the anhydrous phase of stoichiometric hydrates.[41−43] Water infiltration into perovskite-like oxides is a common strategy to enhance proton conductivity.[42,44] The diffusion is possible because of available space or channels in perovskite.[45] In many cases, the infiltration will not change the crystal structure, but will expand the unit cells as observed in our case.[14,46]

It was predicted that the band gap will increase as a result of expanded unit cell,[18,21] but our UV−vis measurement shows no apparent change. Photoluminescence becomes enhanced by several folds upon or after water infiltration (Figure S15), in good agreement with previous observations,[47] but the PL peak position experiences a red shift as opposed to the blue shift observed in single-crystal film.[20] Note that there is no contradiction between UV−vis and photoluminescence because photoluminescence can be affected by many factors; it is not an accurate method to determine band edge positions. Similar to the effect on PL, a large photoconductivity enhancement was also observed upon exposure to 84% RH N_2 (Figure S11). SEM further revealed an increase in the grain size after exposure for 1 h (Figure S10). It is well-known that larger grains can reduce defect states and grain boundaries, thus leading to better device performances.[48−50] The enhanced PL and photoconductivity have been reported in moist treated perovskite, but it is the first time to show that moisture can increase perovskite grain size.

Our observation of stable thin film in ambient conditions or in high humidity agrees well with previous observations by several groups.[15−17] The less stable single-crystal perovskite powder and perovskite from dehydrated monohydrate are due to their porous structures. The single-crystal sample in Figure 3c,d is actually a powder pellet made of microsized particles from large millimeter-sized single crystal for attenuated total reflectance (ATR) FTIR measurement. Such porous structure also makes it easy to trap and absorb water molecules, leading to stronger water absorption in FTIR and degradation to monohydrate. The potential high stability and its dependence on the microstructure, ambient moisture, and light provide new insight into alternative degradation mechanisms and highly stable perovskite solar cells.

MATERIALS AND METHODS

Preparation of $CH_3NH_3PbI_3$ Films, Single Crystals of $CH_3NH_3PbI_3$ and $CH_3NH_3PbI_3{\cdot}H_2O$. $CH_3NH_3PbI_3$ ($MAPbI_3$) films were synthesized based on the methods described in refs 9, 51, and 52. Lead iodide (PbI_2), dimethyl sulfoxide (DMSO), *N*,*N*-dimethylformamide (DMF), isopropanol (IPA), and toluene were purchased from Sigma-Aldrich (St. Louis), and methylammonium iodide (MAI) was purchased from Lumtec (Taiwan, Republic of China). All chemicals were used without further purification. For preparation of PbI_2(DMSO) complex, PbI_2 (5 g) was dissolved in 15 mL of DMSO at 60 °C under stirring and then 35 mL of toluene was dripped into the PbI_2 solution slowly to form white precipitate. The white precipitate was filtered and dried in a vacuum oven at 60 °C for 24 h. The chemical composition of the produced powder was confirmed by XRD. Prepared PbI_2(DMSO) complex was then dissolved in DMF at room temperature. First, the PbI_2(DMSO) complex solution (1.3 M) was spin-coated on a substrate at 3000 rpm for 30 s. MAI solution (70 mg/mL) in IPA was spin-coated on top of the transparent PbI_2(DMSO) film at 5000 rpm for 30 s. Then the film was annealed at 100 °C for 5 min. $MAPbI_3$ and $MAPbI_3$ H_2O single crystals were synthesized following the work of Poglitsch and Weber.[25] For MAPbI3, 2.915 g of lead(II) acetate trihydrate (99%, Alfa Aesar, Haverhill, MA) was added to 10 mL of hydriodic acid (HI) (57% w/w aqueous solution (aq. soln.), stab with 1.5% hypophosphorous acid, Alfa Aesar) in a 50 mL flat bottom flask. The mixed HI acid solution was heated up to 100 °C in a water bath. Two milliliters of HI solution (57% w/w aq. soln., Alfa Aesar) and 1.7 mL of methylamine solution (40% w/w aq. soln., Alfa Aesar) were first mixed in a 10 mL beaker and then added into the hot solution. After 24 h gradual cooling from 100 to 70 °C, black precipitate was obtained on the flask bottom which was then filtered, washed, and dried. In Poglitsch and Weber's work, it was also mentioned that a hydrated form of $MAPbI_3$ can be obtained if the temperature of the solution is lowered below 40 °C. The same method as the preparation of $MAPbI_3$ crystals was used, but the solution was cooled from 100 °C to room temperature in 24 h. After 2 days at room temperature in the dark, pale yellow thin needles were found in the flask. The filtered pale yellow needles are metastable and would turn into polycrystalline $MAPbI_3$ by losing the crystalline water even in ambient environment (25 °C, 45% RH). It was confirmed by XRD that the pale yellow needle is the monohydrate of perovskite, $CH_3NH_3PbI_3{\cdot}H_2O$. Figure S1a in the Supporting Information shows an optical image of $MAPbI_3$ single crystal. Figure S1b,c shows scanning electron microscopy (SEM) images of a surface and cross section of a $MAPbI_3$ film on silicon substrate. Figure S1d−f shows SEM images of $MAPbI_3$ films on different substrates—glass, silicon, and QCM chip, respectively.

Setup for the Generation of Moist N_2. Figure S2 shows the setup to produce moist N_2 with controlled relative humidity (RH) levels. To maintain a stable RH environment, dry N_2 was connected to a mass flow controller with constant flow rate, and moist nitrogen gas was obtained after passing through a flask bubbler which contained deionized water or saturated salt solutions. The RH was measured in real time throughout the experiment using a calibrated hygrometer (±5% margin of error) placed downstream of moist N_2 in the sample chamber.

Fourier Transform Infrared Spectroscopy (FTIR). The FTIR spectra were recorded with a Nicolet iS50 FT-IR Spectrometer using three configurations: (1) a Ge single attenuated total reflection (Ge-sATR) for Figure 1b−d and Figure 3a−d; (2) a ZnSe multiple attenuated total reflection (ZnSe mATR) for Figure 4a and Figure S3;[53] (3) conventional thin film transmission for Figure S4. For $MAPbI_3$ in Figure 3c,d, single-crystal $MAPbI_3$ was ground to microsized powders and then pressed into a pellet on the Ge sATR. The measurements were performed either in the ambient condition with room temperature of ∼25 °C and relative humidity in the range of 40%−45%, or in moist N_2.

First-Principles Calculations. The lattice dynamics and molecular vibration calculations of $MAPbI_3{\cdot}H_2O$ were performed using the density functional perturbation theory.[54] The results closest to the experimental ones were obtained within the generalized-gradient approximation with PBE exchange-correlation functional as implemented in the QUANTUM ESPRESSO suite.[28] The experimental crystal structure of $MAPbI_3{\cdot}H_2O$,[23] space group $P2_1/m$, with a = 10.3939 Å, α = 90.00° b = 4.6419 Å, β = 101.161°, c = 11.1181 Å, and γ = 90.00° was relaxed at fixed lattice parameters. The total energy minimized self-consistently (SCF) with 75 Ry kinetic energy cutoff for the plane wave, 300 Ry charge density cutoff, energy convergence 10^{-10}, and force convergence greater than 10^{-9} over 4 × 8 × 4 Monkhorst−Pack mesh. Figure S5 displays the atomic displacements in the calculated IR active modes with frequencies in the experimentally accessible range 800−4000 cm^{-1}.

Quartz Crystal Microbalance with Dissipation (QCM-D). The QCM-D measurement was performed using Biolin Scientific Q-Sense E1 system equipped with a humidity module. Figure S8 shows the schematics. To monitor the mass change of $MAPbI_3$ film under moisture treatment, the film was spin-coated directly on a QCM-D chip. Figure S9 shows a negligible mass change of a $MAPbI_3$ film in dry N_2 after it was exposed to the ambient air for 10 min. Different salt solutions were used to produce nitrogen with well-controlled relative

DOI: 10.1021/acs.chemmater.6b02883
Chem. Mater. 2016, 28, 7385−7393

humidity. Table S1 shows 5 RH levels from 32% to 97% with five solutions.[55] Table S2 shows that the amount of infiltrated water is proportional to the mass of $MAPbI_3$ film.

Photoconductivity. Gold (50 nm)/chromium (5 nm) contacts were fabricated on precleaned glass substrate by electron-beam deposition. An optic fiber was used as shadow mask. $MAPbI_3$ film was spin-coated on the substrate after contacts deposition. A Keithley 2400 Source-Meter unit was used to characterize the electrical property. The device was illuminated by a 532 nm laser during the photoconductivity measurement. Each device was aged under 532 nm laser illumination in dry N_2 atmosphere for more than 15 min.

Photoluminescence (PL). The PL spectra of $MAPbI_3$ films were measured using a HORIBA iHR320 Spectrometer equipped with Synapse CCD. A 532 nm continuous wave laser was used as an excitation source. The measurements were performed in ambient condition. Figures S10–S13 show PL spectra and intensities of $MAPbI_3$ films in ambient air, dry N_2, and moist N_2.

Powder X-ray Diffraction. Powder X-ray diffractograms were recorded using X'Pert PRO PANalytical X-ray powder diffractometer with Cu Kα radiation (λ = 1.54178 Å). Unit cell refinement for all sample powder X-ray diffractograms were obtained using whole pattern fitting refined with LeBail Method[56] that was inserted in the Jana2006 software package.[57] The same system was used to measure the NIST standard silicon reference with a = 5.431195(9). By application of the same refinement method, the lattice parameter was obtained as a = 5.43158(3). The ambient temperature in the PXRD lab was maintained at ~20 °C all the time. Figure S16 shows XRD patterns of $MAPbI_3$ and $MAPbI_3{\cdot}H_2O$. Figure S17 and Table S3 show the XRD pattern and unit cell parameters obtained from unit cell refinement.

■ ASSOCIATED CONTENT

Supporting Information

The Supporting Information is available free of charge on the ACS Publications website at DOI: 10.1021/acs.chemmater.6b02883.

Images of synthesized $MAPbI_3$ single crystal and thin films, setup for the generation of moist N_2; FTIR spectra of adsorbed water; FTIR transmission spectra of $MAPbI_3$ films coated on double-side polished silicon substrates in vacuum and ambient air; atomic displacements of IR modes in monoclinic $CH_3NH_3PbI_3{\cdot}H_2O$; FTIR spectra of bulk water and perovskite absorbed water; pictures of Ge single-ATR and ZnSe multi-ATR; schematic of QCM-D humidity module; QCM-D measurement of adsorbed water by $MAPbI_3$ thin film exposed to the ambient air; SEM pictures and electronic properties of $MAPbI_3$ films and devices upon exposure to moist N_2 atmosphere; PL spectra of a $MAPbI_3$ film in ambient air and dry N_2; evolution of PL intensities of $MAPbI_3$ film under continuous illumination of a 473 nm laser in ambient air and dry N_2; normalized PL spectra of $MAPbI_3$ film after exposure to dry N_2 for 30 min and then to continuous moist N_2 flow; PL spectra of $MAPbI_3$ film after repeated exposure to dry N_2 moist N_2, experimental and simulated PXRD patterns of $MAPbI_3$ hydrate, $MAPbI_3$ film, and $MAPbI_3$ single-crystal powder; a typical PXRD pattern fitting result (scan #3 in Table S3) obtained using LeBail Method which was inserted in the Jana2006 software package; a list of relative humidity values (RH) for several standard salt solutions at 25 °C; QCM-D results of $MAPbI_3$ films with different initial masses or thicknesses; unit cell refinement results for $CH_3NH_3PbI_3$ thin film powder X-ray diffractograms. All data needed to evaluate the conclusions in the paper are present in the paper and/or the Supporting Information. Additional data related to this paper may be requested from the authors (PDF)

■ AUTHOR INFORMATION

Corresponding Authors

*E-mail: jbao@uh.edu (J.M.B.).
*E-mail: zhmwang@uestc.edu.cn (Z.M.W.)

Funding

J.M.B. acknowledges support from the Robert A. Welch Foundation (E-1728) and the National Science Foundation (Career Award ECCS-1240510). V.G.H. work was supported by the State of Texas through the Texas Center for Superconductivity at the University of Houston (TcSUH). R.G. and W.Z.L. acknowledge support by the National Science Foundation (Grant No. CMMI-1334417 and DMR-1506640). Y.Y. acknowledges the TcSUH award funding. A.M.G. acknowledges the Welch Foundation (E-1297).

Notes

The authors declare no competing financial interest.

■ REFERENCES

(1) Miyasaka, T. Perovskite Photovoltaics: Rare Functions of Organo Lead Halide in Solar Cells and Optoelectronic Devices. *Chem. Lett.* **2015**, *44*, 720–729.
(2) Park, N. G. Perovskite solar cells: an emerging photovoltaic technology. *Mater. Today* **2015**, *18*, 65–72.
(3) Rong, Y. G.; Liu, L. F.; Mei, A. Y.; Li, X.; Han, H. W. Beyond Efficiency: the Challenge of Stability in Mesoscopic Perovskite Solar Cells. *Adv. Energy Mater.* **2015**, *5*, 1501066.
(4) Leijtens, T.; Eperon, G. E.; Noel, N. K.; Habisreutinger, S. N.; Petrozza, A.; Snaith, H. J. Stability of Metal Halide Perovskite Solar Cells. *Adv. Energy Mater.* **2015**, *5*, 1500963.
(5) Berry, J.; Buonassisi, T.; Egger, D. A.; Hodes, G.; Kronik, L.; Loo, Y. L.; Lubomirsky, I.; Marder, S. R.; Mastai, Y.; Miller, J. S.; Mitzi, D. B.; Paz, Y.; Rappe, A. M.; Riess, I.; Rybtchinski, B.; Stafsudd, O.; Stevanovic, V.; Toney, M. F.; Zitoun, D.; Kahn, A.; Ginley, D.; Cahen, D. Hybrid Organic-Inorganic Perovskites (HOIPs): Opportunities and Challenges. *Adv. Mater.* **2015**, *27*, 5102–5112.
(6) Snaith, H. J. Perovskites: The Emergence of a New Era for Low-Cost, High-Efficiency Solar Cells. *J. Phys. Chem. Lett.* **2013**, *4*, 3623–3630.
(7) Niu, G. D.; Guo, X. D.; Wang, L. D. Review of recent progress in chemical stability of perovskite solar cells. *J. Mater. Chem. A* **2015**, *3*, 8970–8980.
(8) Tiep, N. H.; Ku, Z. L.; Fan, H. J. Recent Advances in Improving the Stability of Perovskite Solar Cells. *Adv. Energy Mater.* **2016**, *6*, 1501420.
(9) Kojima, A.; Teshima, K.; Shirai, Y.; Miyasaka, T. Organometal Halide Perovskites as Visible-Light Sensitizers for Photovoltaic Cells. *J. Am. Chem. Soc.* **2009**, *131*, 6050–6051.
(10) Noh, J. H.; Im, S. H.; Heo, J. H.; Mandal, T. N.; Seok, S. I. Chemical Management for Colorful, Efficient, and Stable Inorganic-Organic Hybrid Nanostructured Solar Cells. *Nano Lett.* **2013**, *13*, 1764–1769.
(11) Baikie, T.; Fang, Y. N.; Kadro, J. M.; Schreyer, M.; Wei, F. X.; Mhaisalkar, S. G.; Graetzel, M.; White, T. J. Synthesis and crystal chemistry of the hybrid perovskite $CH_3NH_3PbI_3$ for solid-state sensitised solar cell applications. *J. Mater. Chem. A* **2013**, *1*, 5628–5641.
(12) Niu, G. D.; Li, W. Z.; Meng, F. Q.; Wang, L. D.; Dong, H. P.; Qiu, Y. Study on the stability of $CH_3NH_3PbI_3$ films and the effect of post-modification by aluminum oxide in all-solid-state hybrid solar cells. *J. Mater. Chem. A* **2014**, *2*, 705–710.
(13) Frost, J. M.; Butler, K. T.; Brivio, F.; Hendon, C. H.; van Schilfgaarde, M.; Walsh, A. Atomistic Origins of High-Performance in

DOI: 10.1021/acs.chemmater.6b02883
Chem. Mater. 2016, 28, 7385–7393

Hybrid Halide Perovskite Solar Cells. *Nano Lett.* **2014**, *14*, 2584−2590.
(14) Ahmed, I.; Eriksson, S.; Ahlberg, E.; Knee, C.; Berastegui, P.; Johansson, L.; Rundlof, H.; Karlsson, M.; Matic, A.; Borjesson, L.; Engberg, D. Synthesis and structural characterization of perovskite type proton conducting $BaZr_{1-x}In_xO_{3-delta}$ ($0.0 \leq x \leq 0.75$). *Solid State Ionics* **2006**, *177*, 1395−1403.
(15) Christians, J. A.; Herrera, P. A. M.; Kamat, P. V. Transformation of the Excited State and Photovoltaic Efficiency of $CH_3NH_3PbI_3$ Perovskite upon Controlled Exposure to Humidified Air. *J. Am. Chem. Soc.* **2015**, *137*, 1530−1538.
(16) Yang, J. L.; Siempelkamp, B. D.; Liu, D. Y.; Kelly, T. L. Investigation of $CH_3NH_3PbI_3$ Degradation Rates and Mechanisms in Controlled Humidity Environments Using in Situ Techniques. *ACS Nano* **2015**, *9*, 1955−1963.
(17) Leguy, A. M. A.; Hu, Y.; Campoy-Quiles, M.; Alonso, M. I.; Weber, O. J.; Azarhoosh, P.; van Schilfgaarde, M.; Weller, M. T.; Bein, T.; Nelson, J.; Docampo, P.; Barnes, P. R. F. Reversible Hydration of $CH_3NH_3PbI_3$ in Films, Single Crystals, and Solar Cells. *Chem. Mater.* **2015**, *27*, 3397−3407.
(18) Mosconi, E.; Azpiroz, J. M.; De Angelis, F. Ab Initio Molecular Dynamics Simulations of Methylammonium Lead Iodide Perovskite Degradation by Water. *Chem. Mater.* **2015**, *27*, 4885−4892.
(19) Tong, C. J.; Geng, W.; Tang, Z. K.; Yam, C. Y.; Fan, X. L.; Liu, J.; Lau, W. M.; Liu, L. M. Uncovering the Veil of the Degradation in Perovskite $CH_3NH_3PbI_3$ upon Humidity Exposure: A First-Principles Study. *J. Phys. Chem. Lett.* **2015**, *6*, 3289−3295.
(20) Grancini, G.; D'Innocenzo, V.; Dohner, E. R.; Martino, N.; Kandada, A. R. S.; Mosconi, E.; De Angelis, F.; Karunadasa, H. I.; Hoke, E. T.; Petrozza, A. $CH_3NH_3PbI_3$ perovskite single crystals: surface photophysics and their interaction with the environment. *Chem. Sci.* **2015**, *6*, 7305−7310.
(21) Müller, C.; Glaser, T.; Plogmeyer, M.; Sendner, M.; Döring, S.; Bakulin, A. A.; Brzuska, C.; Scheer, R.; Pshenichnikov, M. S.; Kowalsky, W.; Pucci, A.; Lovrinčić, R. Water Infiltration in Methylammonium Lead Iodide Perovskite: Fast and Inconspicuous. *Chem. Mater.* **2015**, *27*, 7835−7841.
(22) Song, Z.; Abate, A.; Watthage, S. C.; Liyanage, G. K.; Phillips, A. B.; Steiner, U.; Graetzel, M.; Heben, M. J. Perovskite Solar Cell Stability in Humid Air: Partially Reversible Phase Transitions in the PbI_2-CH_3NH_3I-H_2O System. *Adv. Energy Mater.* **2016**, 1600846.
(23) Hao, F.; Stoumpos, C. C.; Liu, Z.; Chang, R. P. H.; Kanatzidis, M. G. Controllable Perovskite Crystallization at a Gas-Solid Interface for Hole Conductor-Free Solar Cells with Steady Power Conversion Efficiency over 10%. *J. Am. Chem. Soc.* **2014**, *136*, 16411−16419.
(24) Imler, G. H.; Li, X.; Xu, B. L.; Dobereiner, G. E.; Dai, H. L.; Rao, Y.; Wayland, B. B. Solid state transformation of the crystalline monohydrate $(CH_3NH_3)PbI_3(H_2O)$ to the $(CH_3NH_3)PbI_3$ perovskite. *Chem. Commun.* **2015**, *51*, 11290−11292.
(25) Poglitsch, A.; Weber, D. Dynamic disorder in methylammoniumtrihalogenoplumbates(ii) observed by millimeter-wave spectroscopy. *J. Chem. Phys.* **1987**, *87*, 6373−6378.
(26) Glaser, T.; Muller, C.; Sendner, M.; Krekeler, C.; Semonin, O. E.; Hull, T. D.; Yaffe, O.; Owen, J. S.; Kowalsky, W.; Pucci, A.; Lovrincic, R. Infrared Spectroscopic Study of Vibrational Modes in Methylammonium Lead Halide Perovskites. *J. Phys. Chem. Lett.* **2015**, *6*, 2913−2918.
(27) Onoda-yamamuro, N.; Matsuo, T.; Suga, H. Calorimetric and IR spectroscopic studies of phase-transitions in methylammonium trihalogenoplumbates-(ii). *J. Phys. Chem. Solids* **1990**, *51*, 1383−1395.
(28) Giannozzi, P.; Baroni, S.; Bonini, N.; Calandra, M.; Car, R.; Cavazzoni, C.; Ceresoli, D.; Chiarotti, G. L.; Cococcioni, M.; Dabo, I.; Dal Corso, A.; de Gironcoli, S.; Fabris, S.; Fratesi, G.; Gebauer, R.; Gerstmann, U.; Gougoussis, C.; Kokalj, A.; Lazzeri, M.; Martin-Samos, L.; Marzari, N.; Mauri, F.; Mazzarello, R.; Paolini, S.; Pasquarello, A.; Paulatto, L.; Sbraccia, C.; Scandolo, S.; Sclauzero, G.; Seitsonen, A. P.; Smogunov, A.; Umari, P.; Wentzcovitch, R. M. QUANTUM ESPRESSO: a modular and open-source software project for quantum simulations of materials. *J. Phys.: Condens. Matter* **2009**, *21*, 395502.
(29) Nie, W.; Blancon, J. C.; Neukirch, A. J.; Appavoo, K.; Tsai, H.; Chhowalla, M.; Alam, M. A.; Sfeir, M. Y.; Katan, C.; Even, J.; Tretiak, S.; Crochet, J. J.; Gupta, G.; Mohite, A. D. Light-activated photocurrent degradation and self-healing in perovskite solar cells. *Nat. Commun.* **2016**, *7*, 11574.
(30) Bryant, D.; Aristidou, N.; Pont, S.; Sanchez-Molina, I.; Chotchunangatchaval, T.; Wheeler, S.; Durrant, J. R.; Haque, S. A. Light and oxygen induced degradation limits the operational stability of methylammonium lead triiodide perovskite solar cells. *Energy Environ. Sci.* **2016**, *9*, 1655−1660.
(31) Prasad, P. S. R.; Chaitanya, V. K.; Prasad, K. S.; Rao, D. N. Direct formation of the gamma-$CaSO_4$ phase in dehydration process of gypsum: In situ FTIR study. *Am. Mineral.* **2005**, *90*, 672−678.
(32) Knop, O.; Wasylishen, R. E.; White, M. A.; Cameron, T. S.; Van Oort, M. J. M. Alkylammonium lead halides. Part 2. $CH_3NH_3PbCl_3$, $CH_3NH_3PbBr_3$, $CH_3NH_3PbI_3$ perovskites - cuboctahedral halide cages with isotropic cation reorientation. *Can. J. Chem.* **1990**, *68*, 412−422.
(33) Wasylishen, R. E.; Knop, O.; Macdonald, J. B. Cation rotation in methylammonium lead halides. *Solid State Commun.* **1985**, *56*, 581−582.
(34) Leguy, A. M. A.; Frost, J. M.; McMahon, A. P.; Sakai, V. G.; Kochelmann, W.; Law, C. H.; Li, X. E.; Foglia, F.; Walsh, A.; O'Regan, B. C.; Nelson, J.; Cabral, J. T.; Barnes, P. R. F. The dynamics of methylammonium ions in hybrid organic-inorganic perovskite solar cells. *Nat. Commun.* **2015**, *6*, 7124.
(35) Motta, C.; El-Mellouhi, F.; Kais, S.; Tabet, N.; Alharbi, F.; Sanvito, S. Revealing the role of organic cations in hybrid halide perovskite $CH_3NH_3PbI_3$. *Nat. Commun.* **2015**, *6*, 7026.
(36) Max, J. J.; Chapados, C. Aqueous ammonia and ammonium chloride hydrates: Principal infrared spectra. *J. Mol. Struct.* **2013**, *1046*, 124−135.
(37) Cziczo, D. J.; Abbatt, J. P. D. Infrared observations of the response of NaCl, $MgCl_2$, NH_4HSO_4, and NH_4NO_3 aerosols to changes in relative humidity from 298 to 238 K. *J. Phys. Chem. A* **2000**, *104*, 2038−2047.
(38) Hatch, C. D.; Wiese, J. S.; Crane, C. C.; Harris, K. J.; Kloss, H. G.; Baltrusaitis, J. Water Adsorption on Clay Minerals As a Function of Relative Humidity: Application of BET and Freundlich Adsorption Models. *Langmuir* **2012**, *28*, 1790−1803.
(39) Sun, Q. Raman spectroscopic study of the effects of dissolved NaCl on water structure. *Vib. Spectrosc.* **2012**, *62*, 110−114.
(40) Auer, B. M.; Skinner, J. L. IR and Raman spectra of liquid water: Theory and interpretation. *J. Chem. Phys.* **2008**, *128*, 224511.
(41) Ortiz, A. U.; Freitas, A. P.; Boutin, A.; Fuchs, A. H.; Coudert, F. X. What makes zeolitic imidazolate frameworks hydrophobic or hydrophilic ? The impact of geometry and functionalization on water adsorption. *Phys. Chem. Chem. Phys.* **2014**, *16*, 9940−9949.
(42) Braun, D. E.; Koztecki, L. H.; McMahon, J. A.; Price, S. L.; Reutzel-Edens, S. M. Navigating the Waters of Unconventional Crystalline Hydrates. *Mol. Pharmaceutics* **2015**, *12*, 3069−3088.
(43) Ma, Q. X.; He, H.; Liu, C. Hygroscopic properties of oxalic acid and atmospherically relevant oxalates. *Atmos. Environ.* **2013**, *69*, 281−288.
(44) Fischer, W.; Reck, G.; Schober, T. Structural transformation of the oxygen and proton conductor $Ba_2In_2O_5$ in humid air: An in-situ X-ray powder diffraction study. *Solid State Ionics* **1999**, *116*, 211−215.
(45) Dang, Y. Y.; Liu, Y.; Sun, Y. X.; Yuan, D. S.; Liu, X. L.; Lu, W. Q.; Liu, G. F.; Xia, H. B.; Tao, X. T. Bulk crystal growth of hybrid perovskite material $CH_3NH_3PbI_3$. *CrystEngComm* **2015**, *17*, 665−670.
(46) Omata, T.; Fuke, T.; Otsuka-Yao-Matsuo, S. Hydration behavior of $Ba_2Sc_2O_5$ with an oxygen-deficient perovskite structure. *Solid State Ionics* **2006**, *177*, 2447−2451.
(47) Eperon, G. E.; Habisreutinger, S. N.; Leijtens, T.; Bruijnaers, B. J.; van Franeker, J. J.; Dequilettes, D. W.; Pathak, S.; Sutton, R. J.; Grancini, G.; Ginger, D. S.; Janssen, R. A. J.; Petrozza, A.; Snaith, H. J. The Importance of Moisture in Hybrid Lead Halide Perovskite Thin Film Fabrication. *ACS Nano* **2015**, *9*, 9380−9393.
(48) You, J. B.; Yang, Y. M.; Hong, Z. R.; Song, T. B.; Meng, L.; Liu, Y. S.; Jiang, C. Y.; Zhou, H. P.; Chang, W. H.; Li, G.; Yang, Y.

DOI: 10.1021/acs.chemmater.6b02883
Chem. Mater. 2016, 28, 7385−7393

Moisture assisted perovskite film growth for high performance solar cells. *Appl. Phys. Lett.* **2014**, *105*, 183902.
(49) Nie, W. Y.; Tsai, H. H.; Asadpour, R.; Blancon, J. C.; Neukirch, A. J.; Gupta, G.; Crochet, J. J.; Chhowalla, M.; Tretiak, S.; Alam, M. A.; Wang, H. L.; Mohite, A. D. High-efficiency solution-processed perovskite solar cells with millimeter-scale grains. *Science* **2015**, *347*, 522−525.
(50) Pathak, S.; Sepe, A.; Sadhanala, A.; Deschler, F.; Haghighirad, A.; Sakai, N.; Goedel, K. C.; Stranks, S. D.; Noel, N.; Price, M.; Huttner, S.; Hawkins, N. A.; Friend, R. H.; Steiner, U.; Snaith, H. J. Atmospheric Influence upon Crystallization and Electronic Disorder and Its Impact on the Photophysical Properties of Organic-Inorganic Perovskite Solar Cells. *ACS Nano* **2015**, *9*, 2311−2320.
(51) Rong, Y. G.; Tang, Z. J.; Zhao, Y. F.; Zhong, X.; Venkatesan, S.; Graham, H.; Patton, M.; Jing, Y.; Guloy, A. M.; Yao, Y. Solvent engineering towards controlled grain growth in perovskite planar heterojunction solar cells. *Nanoscale* **2015**, *7*, 10595−10599.
(52) Yang, W. S.; Noh, J. H.; Jeon, N. J.; Kim, Y. C.; Ryu, S.; Seo, J.; Seok, S. I. High-performance photovoltaic perovskite layers fabricated through intramolecular exchange. *Science* **2015**, *348*, 1234−1237.
(53) Liu, Z. H.; Lu, X. X.; Peng, P.; Wu, W.; Pei, S. S.; Yu, Q. K.; Bao, J. M. Room-temperature Fano resonance tunable by chemical doping in few-layer graphene synthesized by chemical-vapor deposition. *Phys. Rev. B: Condens. Matter Mater. Phys.* **2010**, *82*, 155435.
(54) Baroni, S.; de Gironcoli, S.; Dal Corso, A.; Giannozzi, P. Phonons and related crystal properties from density-functional perturbation theory. *Rev. Mod. Phys.* **2001**, *73*, 515−562.
(55) Greenspan, L. Humidity fixed-points of binary saturated aqueous-solutions. *J. Res. Natl. Bur. Stand., Sect. A* **1977**, *81*, 89−96.
(56) Le Bail, A. Whole powder pattern decomposition methods and applications: A retrospection. *Powder Diffr.* **2005**, *20*, 316−326.
(57) Petricek, V.; Dusek, M.; Palatinus, L. Crystallographic Computing System JANA2006: General features. *Z. Kristallogr. - Cryst. Mater.* **2014**, *229*, 345−352.

DOI: 10.1021/acs.chemmater.6b02883
Chem. Mater. 2016, 28, 7385−7393